Langmuir

Article

pubs.acs.org/Langmuir

Temperature-Dependent Infrared and Calorimetric Studies on Arsenicals Adsorption from Solution to Hematite Nanoparticles

Md Abdus Sabur,[†] Sabine Goldberg,[‡] Adrian Gale,[§] Nadine Kabengi,[§] and Hind A. Al-Abadleh*,[†]

[†]Department of Chemistry and Biochemistry, Wilfrid Laurier University, Waterloo, ON N2L 3C5, Canada

[‡]U.S. Salinity Laboratory, USDA-ARS, Riverside, California 92507, United States

[§]Department of Geoscience, Georgia State University, Atlanta, Georgia 30303, United States

Supporting Information

ABSTRACT: To address the lack of systematic and surface sensitive studies on the adsorption energetics of arsenic compounds on metal (oxyhydr)oxides, we conducted temperature-dependent ATR-FTIR studies for the adsorption of arsenate, monomethylarsonic acid, and dimethylarsinic acid on hematite nanoparticles at pH 7. Spectra were collected as a function of concentration and temperature in the range 5−50 °C (278−323 K). Adsorption isotherms were constructed from spectral features assigned to surface arsenic. Values of K_{eq}, adsorption enthalpy, and entropy were extracted from fitting the Langmuir model to the data and from custom-built triple-layer surface complexation models derived from our understanding of the adsorption mechanism of each arsenical. These spectroscopic and modeling results were complemented with flow-through calorimetric measurements of molar heats of adsorption. Endothermic adsorption processes were predicted from the application of mathematical models with a net positive change in adsorption entropy. However, experimentally measured heats of adsorption were exothermic for all three arsenicals studied herein, with arsenate releasing 1.6−1.9 times more heat than methylated arsenicals. These results highlight the role of hydration thermodynamics on the adsorption of arsenicals, and are consistent with the spectral interpretation of type of surface complexes each arsenical form in that arsenate is mostly dominated by bidentate, MMA by a mixture of mono- and bidentate, and DMA by mostly outer sphere.

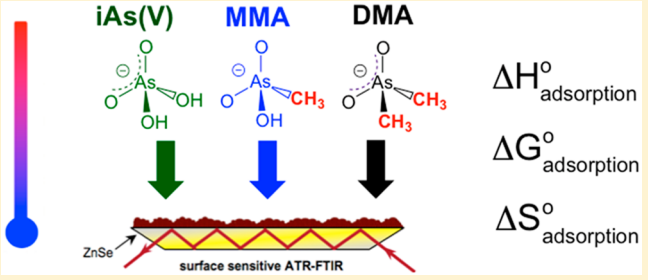

INTRODUCTION

The surface chemistry of arsenic compounds with reactive components in soils and remediation technologies continues to be of interest to scientists because it impacts their transport, bioavailability, and concentration in potential drinking water sources.[1,2] As an element that exists naturally in many rocks and minerals around the world, natural weathering and changes to redox and chemical conditions surrounding the rocks liberate arsenic from the solid phase. Also, the level of microbial activities in surface water and soils drives the cycling of arsenic compounds between inorganic arsenate and methylated forms, monomethylarsonic acid (MMA) and dimethylarsinic acid (DMA).[3,4] Anthropogenic activities that introduce arsenic into the environment are mainly mining and burning of fossil fuels.[5] In addition, arsenic-containing semiconducting materials such as gallium arsenate show promising performance in electronic devices and solar cells.[6] On the consumer scale, it is projected that the manufacturing and disposal of arsenic-containing solid waste (if not treated) would elevate arsenic concentrations above background levels in waters and soils.[2]

At a molecular level, arsenate and methylated arsenicals are negatively charged oxyanions whose adsorption on the positively charged sites of metal (oxyhydr)oxides is largely driven by electrostatics.[7] The ligand exchange process that takes place at the interface not only modifies net surface charge but also releases weaker ligands such as protons, carbonate, metal cations, and organic matter. Hence, quantifying adsorption energetics of arsenic compounds has been the subject of a number of batch and surface-sensitive studies, in addition to molecular modeling using density functional theory (DFT) (see refs 8−10 for literature reviews). Experimentally, Gibbs free energies of adsorption (ΔG°_{ads}) are calculated from binding affinity constants, K_{eq}. These values are extracted from applying the Langmuir adsorption model, or a surface complexation model to room-temperature isotherm data at a given pH, or pH edge data at a given bulk phase concentration. These studies are useful in quantifying the effect of factors such as pH, ionic strength, type of adsorbent, and organic substituents on arsenate. While these studies have shown that ligand exchange of arsenic compounds with metal (oxyhydr)oxides is spontaneous, they cannot be used to estimate heat of adsorption, ΔH°_{ads}, or changes to adsorption entropy, ΔS°_{ads}.

To answer the question of whether adsorption of arsenic compounds is enthalpy- or entropy-driven, few batch

Received: November 26, 2014
Revised: January 16, 2015
Published: February 19, 2015

DOI: 10.1021/la504581p
Langmuir 2015, 31, 2749−2760

adsorption studies were conducted for arsenate as a function of temperature, typically from 293 to 338 K.[11−14] Values of temperature-dependent K_{eq} were extracted from fitting the experimental data to the Langmuir model or other empirical models. Tuna et al. reported an exothermic reaction (−52 kJ mol^{-1}) accompanied by a decrease in entropy (−0.084 kJ K^{-1} mol^{-1}) using a hybrid Fe(III)-activated carbon adsorbent at pH 3.[11] In another study, Partey et al.[12] reported an endothermic adsorption reaction for arsenate (17.8 kJ mol^{-1}) on laterite iron concretions, which contain a mixture of iron, manganese, titanium, and aluminum (oxyhydr)oxides, with a net positive change in entropy (+0.033 kJ K^{-1} mol^{-1}) at pH 7. For experiments on iron oxide/silica adsorbent (Fe/Si = 3), Zeng reported exothermic arsenate adsorption (−32 kJ mol^{-1}) with a net positive change in entropy (+0.013 kJ K^{-1} mol^{-1}).[13] Similar results were found in batch isotherm temperature-dependent studies of phosphate adsorption on soils as critically analyzed by Harvey and Rhue.[14]

Direct measurement of reaction heat for surface reactions has been possible through flow adsorption calorimetry.[15] For example, Kabengi et al.[16] reported a range of values, from −3 to −66 kJ mol^{-1}, for arsenate adsorption on amorphous aluminum hydroxide at pH 5.7. Using the same technique, Harvey and Rhue reported exothermic adsorption of phosphate on a multicomponent Al(III)−Fe(III) hydroxide system, with molar heats between −25 and −39 kJ mol^{-1} at pH 4.8.[14] Moreover, using isothermal titration calorimetry, Penn and co-workers quantified heat of reaction as phosphate solutions were titrated with kaolinite[17] and different types of soils.[18] For the former, at pH 4.3, initial fast exothermic reactions were followed by slower endothermic ones, whereas only exothermic reactions were observed at pH 6.3. Multiple titrations of the soil samples exhibited endo- and exothermic patterns, which were interpreted as surface precipitation for the former and ligand exchange for the latter. Earlier, Miltenburg and Golterman[19] measured exothermic enthalpy of phosphate adsorption on ferric hydroxide in the presence and absence of buffer. In all of the above studies, the authors relied on the interpretation of infrared and X-ray spectroscopic data that provide structural details on the nature of surface complexes. Hence, for calorimetric measurements to be contextual, they have to be coupled with results from other techniques.

To address the lack of systematic and surface sensitive studies on the adsorption energetics of arsenic compounds on metal (oxyhydr)oxides, we conducted herein temperature-dependent ATR-FTIR studies on the adsorption of arsenate, MMA, and DMA on hematite nanoparticles at pH 7. Spectra were collected as a function of concentration and temperature in the range 5−50 °C (278−323 K). To our knowledge, these are the first temperature-dependent infrared spectra to be recorded for surface arsenic compounds. These spectroscopic and modeling results were complemented with flow-through calorimetric measurements of molar heats of adsorption. As detailed below, this integrated approach proved invaluable in providing a comprehensive picture of the effect of organic substitution on the adsorption energetics of arsenate on hematite.

EXPERIMENTAL SECTION

Chemicals. Arsenicals used in this study include arsenate (sodium hydrogen arsenate heptahydrate, $Na_2HAsO_4{\cdot}7H_2O$, ACS reagent, J.T. Baker, used as received), MMA (disodium methyl arsonate hexahydrate, $CH_3AsNa_2O_3{\cdot}6H_2O$, 97.5%, Chem Service Inc., used as received), and DMA (sodium cacodylate trihydrate, $C_2H_6AsO_2Na{\cdot}3H_2O$, 98%, Sigma-Aldrich, used as received). *Caution: the aforementioned arsenical compounds are highly toxic via inhalation and skin contact and are carcinogens.* Table S1 shows the structure and pK_a values of these compounds. Aqueous phase solutions of arsenic compounds in the concentration range 0.005−1 mM were prepared by dissolving the respective compound in 0.01 M NaCl background solution (from crystalline solid, 99%, ACS reagent, BDH). Millipore water (18 MΩ·cm) was used and adjusted to pH 7 using NaOH (from pellets, ACS grade, 99.0−100%, EMD) and HCl (6 N, Ricca Chemical). For experiments conducted in D_2O, the following chemicals were used in preparing arsenic solutions in a glovebox purged with dry air (RH < 1%): D_2O (deuterium oxide, 99.9 atom % D, Sigma-Aldrich), DCl (deuterium chloride solution, 35 wt % in D_2O, 99 atom % D, Sigma-Aldrich), NaOD (sodium deuteroxide, 40 wt % in D_2O, 99.5 atom % D, Sigma-Aldrich), and pHydrion Trichek buffer capsule set (pH = 4.00 ± 0.02, 7.00 ± 0.02, and 10.00 ± 0.02, Micro Essential Laboratory, USA). Hematite nanoparticles were used in the adsorption experiments (α-Fe_2O_3, >99.9%, nanostructured and amorphous materials, 19 m^2/g surface area, 67 nm average diameter, and 8.6 isoelectric point). This material was used previously in our lab for adsorption isotherm, pH envelope, and kinetic experiments.[8,20] Details on film preparation are in the Supporting Information.

ATR-FTIR Spectroscopy Experiments. For each isotherm experiment, arsenical solutions were flowed from lower to higher concentrations across the freshly prepared hematite film for 15 min for each concentration. Earlier kinetic studies[8] showed no appreciable change in the intensity of spectral features after that time. ATR-FTIR single beam spectra were collected as a function of concentration on a freshly prepared film using a HATRPlus accessory (Pike Technologies) installed in a Nicolet 8700 FTIR spectrometer (Thermo Instruments) equipped with an MCT-A detector. The ATR flow cell contains a 60° ZnSe crystal IRE (80 × 10 × 4 mm, 100 μL). Spectra were collected at 8 cm^{-1} resolution with 100 averaged scans. At the beginning of every experiment, the NaCl solution was flowed first for 90 min to record background spectra, and then arsenical solutions were flowed one after another over the same film. Flow rate for all the solutions was maintained at 2 mL/min using Tygon tubes (0.8 mm i.d., Masterflex) and a compact pump (Masterflex L/S). Each single beam spectrum collected at the end of passing every arsenical solution at a given concentration was referenced to the last one recorded for the background solution to obtain the absorbance spectra reported herein. All the experiments were repeated at least twice under the same experimental conditions to determine the precisions of our experiments.

Adsorption isotherm experiments for each arsenical were carried out at five temperatures: 5, 15, 25, 35, and 50 °C. The temperature for each experiment was maintained by circulating water from an endocal refrigerated circulating bath (Neslab, RTE-5DD) through the flow channel constructed inside the cover of the ATR flow cell. A thermocouple probe (6 in., Chromega-Alomega, Omega Engineering) was taped using a thermocouple adhesive pad (Omega Engineering) to the top of the ATR flow cell to monitor the temperature throughout the experiment using a temperature reader (ATC-024-1, Harrick Scientific Products, Inc.). Calculations of surface coverage on porous hematite films from ATR-FTIR spectra are described in the Supporting Information (Section 2 and Table S2).

Moreover, bulk phase and adsorption experiments were conducted for arsenate and MMA at room temperature (23 ± 2 °C) using D_2O as a function of pD. For the former, a single beam spectrum was collected first for the background solution (0.01 M KCl in D_2O at pD 7). This was followed by flowing the arsenical solution of interest at a rate of 1 mL/min for 10 min before collecting a single beam spectrum by averaging 300 scans. For the adsorption experiments, a single beam spectrum was collected first after flowing 0.01 M KCl in D_2O for 30 min over a freshly prepared film at a rate of 1 mL/min. Then, the flow of the first arsenical solution started at pD 10, and a spectrum was collected by averaging 300 scans after 10 min of surface interactions. This was followed by the flow of subsequent solutions at pD 8, 5, and 4.

DOI: 10.1021/la504581p
Langmuir 2015, 31, 2749−2760

Surface Complexation Modeling. The triple-layer surface complexation model (SCM) was used to extract values for the adsorption equilibrium constant, K, as a function of temperature for all arsenicals studied herein. The following surface complexation equilibrium reactions were considered for the formation of inner-sphere bidentate arsenate, inner-sphere mono- and bidentate MMA complexes, and simultaneous inner- and outer-sphere monodentate DMA complexes:

$$2FeOH + H_3AsO_4 \rightleftharpoons Fe_2HAsO_4 + 2H_2O \quad (1)$$

$$2FeOH + H_2AsO_3CH_3 \rightleftharpoons Fe_2AsO_3CH_3 + 2H_2O \quad (2)$$

$$FeOH + H_2AsO_3CH_3 \rightleftharpoons FeHAsO_3CH_3 + H_2O \quad (3)$$

$$2FeOH + HAsO_2(CH_3)_2 \rightleftharpoons FeOHFeAsO_2(CH_3)_2 + H_2O \quad (4)$$

$$FeOH + HAsO_2(CH_3)_2 \rightleftharpoons FeOH_2^+ - AsO_2(CH_3)_2^- + H_2O \quad (5)$$

Scheme 1 shows pictorial representations of arsenical surface complexes. Mathematical expressions of K for the above surface complexation reactions are listed in the Supporting Information (Section 3).

Scheme 1. Structure of Surface Complexes in the Ligand Exchange Reactions of Arsenicals

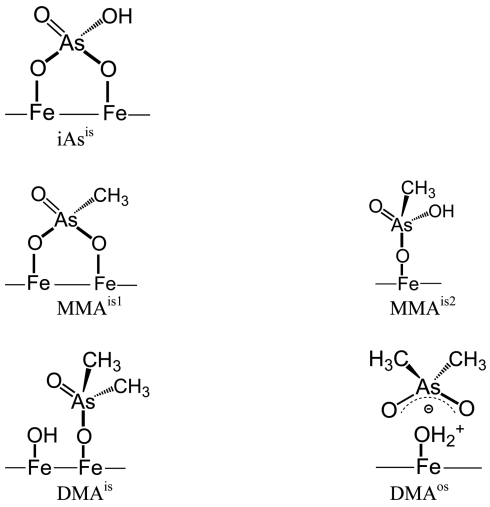

The SCM used herein contain additional reactions and mathematical expressions that describe the clean surface and arsenic species in the bulk as shown in the Supporting Information along with the mass balance equations for the surface functional groups. The computer program FITEQL 4.0 was used to fit the arsenate, MMA, and DMA surface complexation constants to the experimental adsorption data. The FITEQL code fits equilibrium constants to experimental data using a nonlinear least-squares optimization routine and contains the triple-layer model. Parameters were fixed at the following values corresponding to 25 °C: log K_+(int) = 4.3, log K_-(int) = −9.8, log K_{Na+}(int) = −9.3, log K_{Cl-}(int) = 5.4, C_1 = 1.2 F m^{-2}, C_2 = 0.2 F m^{-2} used previously in our description of DMA and *p*-arsanilic acid adsorption on the same hematite.[20] These values change slightly as a function of temperature as shown in Table S3. Estimation of the variance and standard deviation of the fitting parameters was done by propagating the variance in the experimental data according to the detailed description provided in the FITEQL manual.[21]

Calorimetric Measurements. The flow adsorption microcalorimeter (FAMC) used in this study was custom-designed and constructed in-house. A description of the instrumentation and operation of the FAMC has been detailed previously.[16] Only a brief description outlining the basic principles of obtaining data and experimental procedures relevant to this study is provided in the Supporting Information (Section 5). These calorimetric measurements were followed by heats of Cl^- and NO_3^- exchange as well, which provide qualitative insights into the reversibility/irreversibility of arsenic sorption and characterization of surface positive charge.

RESULTS AND DISCUSSION

ATR-FTIR Spectra of Arsenicals Adsorbed on Hematite as a Function of Temperature. Figure 1 shows the ATR-FTIR spectra of adsorbed arsenate, MMA, and DMA as a function of concentration at 5, 25, and 50 °C. Similar spectra were also collected at 15 and 35 °C as shown in the Supporting Information (Figure S2). These spectra were collected while continuously flowing the aqueous phase solutions containing the arsenical at pH 7. The spectral range shown in Figure 1 contains features assigned to the stretching vibrations of As−O bonds, ν(As−O). All these spectra were recorded at concentrations below the detection limit of the ATR crystal to *aqueous phase species* (around 5 mM for arsenate and 8 mM for MMA and DMA at pH 7). Hence, the broad bands shown are due to surface complexes of arsenicals. For adsorbed arsenate, there is little effect of temperature on the spectral intensities and shape of the broad bands with increasing concentration. The pH of our experiments is lower than the PZC of hematite,[8] and hence surface sites are mostly positively charged. Also, at this pH, there are nearly equal aqueous concentration of $HAsO_4^{2-}$ and $H_2AsO_4^-$. The assignment of the most pronounced features at 875 and 795 cm^{-1} is provided below based on earlier IR studies on a number of metal (oxyhydr)oxides that include hematite.[22−27] These studies were coupled with X-ray absorption results suggesting that arsenate forms predominantly inner-sphere bidentate binuclear complexes, which gives rise to ν(As−OFe) in the range 824−800 cm^{-1}.[22−26] The formation of inner-sphere monodentate complexes involved in hydrogen bonding with neighboring sites was also reported as a function of pH by Loring et al.[27] Values of ν(As−O) in these complexes range from 860 to 780 cm^{-1} for singly protonated monodentate complexes around neutral pH, and from 885 to 810 cm^{-1} for doubly protonated monodentate complexes under acidic pH (less than 3). The lowest frequency in the above spectral ranges is assigned to ν(As−OH) in these protonated complexes, which is in general weaker in intensity than features located ≥800 cm^{-1}. Simultaneous formation of inner- and outer-sphere complexes of adsorbed arsenate was reported by Catalano et al.[26] at pH 5, where the latter can give rise to ν(As−O) in the range 861−854 cm^{-1} due to weak interactions with −FeOH sites.[24]

Based on the above, the broad absorption in the range 800−900 cm^{-1} (top panel, Figure 1) composed of a number of overlapping bands, with the most pronounced at 875 cm^{-1}, is assigned to uncomplexed ν(As═O) with a bond order of 1.5 due to resonance, or ν(As−O) weakly H-bonded to neighboring −FeOH sites. The feature at 795 cm^{-1} is assigned to ν(As−OFe) from the formation of a mixture of mono- and bidentate inner sphere. Protonated complexes containing As−OH bonds give rise to ν(As−OH) below 780 cm^{-1}.[22] The formation of outer-sphere complexes cannot be excluded, which will contribute to features above 850 cm^{-1}.

To further verify this spectral assignment, we collected spectra using D_2O at room temperature for aqueous phase and adsorbed arsenate to suppress absorptions due to the liberational mode of water molecules and the bending mode of Fe−OH groups. Figure S3 and Figure 2 (left) show absorption spectra of aqueous phase and adsorbed arsenate as a

DOI: 10.1021/la504581p
Langmuir 2015, 31, 2749−2760

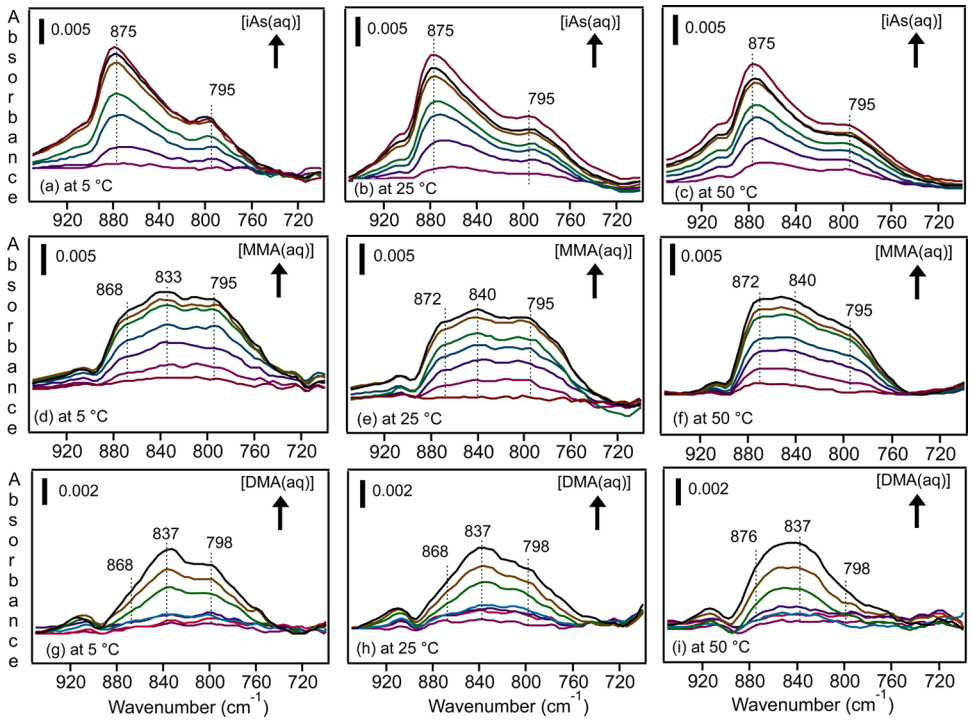

Figure 1. Representative ATR-FTIR absorbance spectra of adsorbed arsenate, MMA, and DMA on hematite nanoparticles at 5, 25, and 50 °C as a function of increasing concentration (from bottom): 0.005, 0.01, 0.03, 0.05, 0.25, 0.5, and 1 mM at pH 7 and I = 0.01 M NaCl.

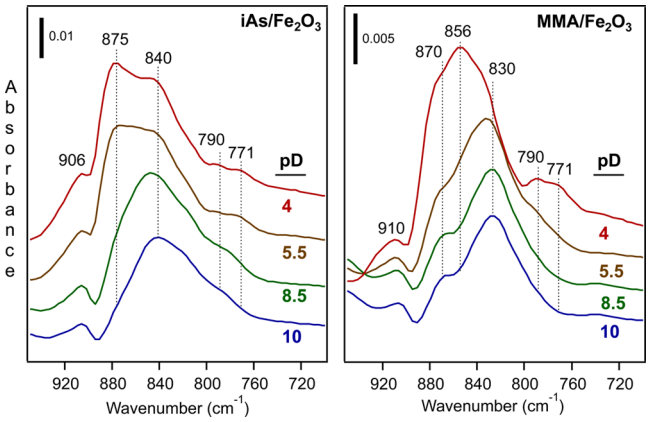

Figure 2. Representative ATR-FTIR absorbance spectra of adsorbed arsenate and MMA on hematite nanoparticles at 25 °C collected in D_2O as a function of decreasing pD. Spectra were collected after 10 min of flowing 0.5 mM of each arsenical.

function of pD, respectively. Features above 800 cm^{-1} assigned to ν(As−O) for different arsenate species in D_2O are similar to those collected earlier in H_2O,[28] namely the red-shift of the most intense feature due to the overall increase in intensity with more deprotonation. In Figure S3 (left), the weak and broad feature at 740 cm^{-1} assigned to ν(As−OD) is more pronounced at pD 5 and is below detection limit for pD 9. There is a slight red-shift in this mode upon deuteration relative to 744 cm^{-1} observed for singly deprotonated arsenate in H_2O.[28] For spectra shown in Figure 2 (left), at pD 10, arsenate inner-sphere complexes are deprotonated giving rise to the 840 cm^{-1} peak assigned to uncomplexed ν(As═O) and the 790 and 771 cm^{-1} components due to ν(As−OFe). With decreasing pD, a high-frequency feature around 875 cm^{-1} increases in intensity, which is observed in the top panel of Figure 1 at pH 7. In the case of bidentate arsenate, protonation of one uncomplexed As−O bond strengthens the double bond character of the neighboring uncomplexed As−O bond. The persistence of the 840 cm^{-1} peak under acidic conditions in our experiments suggests the coexistence of monodentate complexes, which upon formation of one As−OH(D) bond, still contain two uncomplexed As−O bonds in resonance. Loring et al.[27] observed that fully protonated monodentate arsenate complexes on goethite become dominant at pD ≤ 3, which we did not reach in our experiments.

Moreover, we recently ran desorption kinetic studies using aqueous phase phosphate on hematite nanoparticles with preadsorbed arsenate.[30] Results from initial times of surface interactions show that phosphate adsorbs slower by a factor of 6 on hematite surfaces with preadsorbed arsenate than clean surfaces and those with preadsorbed DMA. Also, arsenate desorbs slower by a factor of 7 than DMA, which as explained below, is dominated by weaker monodentate and outer-sphere surface complexation. While the spectral features shown in Figure 1 suggest simultaneous formation of mono- and bidentate complexes for arsenate, it could be inferred from the above analysis that the number of bidentate complexes exceeds that of monodentate.

The middle panel in Figure 1 shows absorbance spectra of adsorbed MMA as a function of concentration and temperature. Increasing the temperature does not cause significant changes to the intensities of the spectral features up to 50 °C. At this highest temperature, the intensity of the high-frequency component at 872 cm^{-1} increases, while that at low frequency (at 795 cm^{-1}) decreases. At pH 7, the aqueous phase is composed of ca. 95% of the singly deprotonated, $CH_3AsO_3H^-$, species. We reported earlier the ATR-FTIR absorbance spectrum of this species at pH 6 and room temperature, which shows an intense spectral band with components at 879 and 866 cm^{-1} assigned to ν(As═O) due to resonance.[28] The

DOI: 10.1021/la504581p
Langmuir 2015, 31, 2749−2760

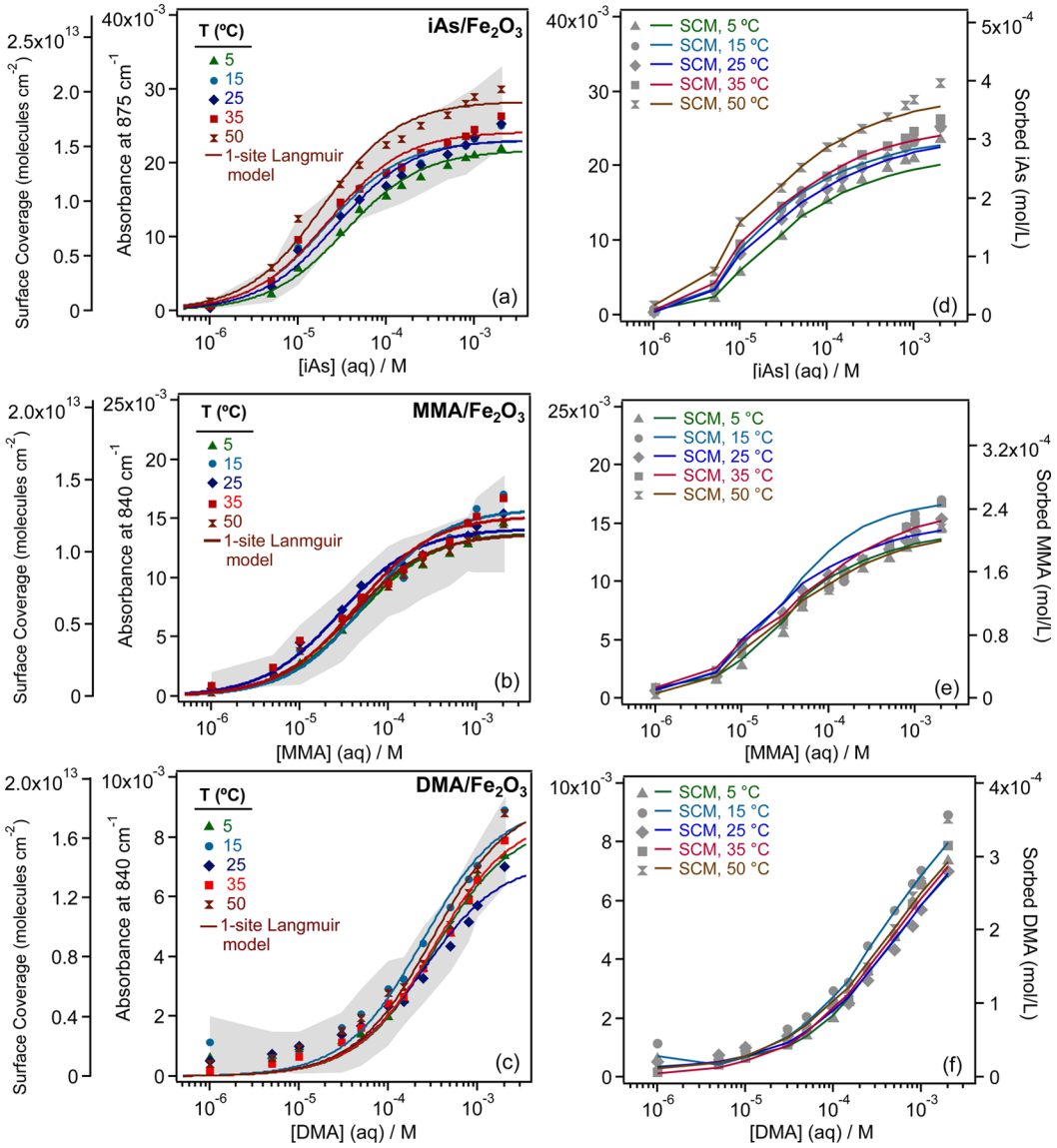

Figure 3. Experimental adsorption isotherms of arsenate, MMA, and DMA on hematite nanoparticles as a function of temperature (filled markers) at pH 7 and 0.01 M NaCl. The solid lines in the left and right panels represent the least-squares fittings of the 1-site Langmuir adsorption model and the triple-layer SCM, respectively. The shaded area represents the uncertainty in the experimental data ($\pm\sigma$) from averaging 2−4 experiments at each temperature, each on a freshly prepared hematite film.

spectrum also shows a weak and broad feature centered at 719 cm^{-1} assigned to ν(As−OH). Complete deprotonation causes a red-shift and splitting in the most intense spectral features due to the formation of ν(As═O) and ν(As−O^-) groups. In the fully protonated MMA species, ν(As═O) appears most intensely at 912 cm^{-1}, with a similar intensity band around 760 cm^{-1}. For comparison, Figure S3 (right) shows absorption spectra of MMA(aq) as a function of pD. Similar to the aforementioned discussion on arsenate, the most intense features above 800 cm^{-1} are red-shifted with increasing deprotonation. The weak and broad feature at 756 cm^{-1} assigned to ν(As−OD) at pD 3 is slightly red-shifted upon deuteration relative to 760 cm^{-1} observed in H_2O.[28]

In the presence of hematite film, spectra of adsorbed MMA were collected at room temperature as a function of pD as shown in Figure 2 (right). At pD 10, features are observed at 830 and 870 cm^{-1}, with the possibility of a low frequency component at 790 cm^{-1}. These features indicate inner-sphere formation, which is very likely to be mostly monodentate guided by spectra shown in Figure S3 (right) at pD 7 and 10. Decreasing pD increases the intensity of the feature at 790 and 771 cm^{-1}, indicating an increase in the surface coverage of inner-sphere complexes or intercomplex conversion from mono- to bidentate complexes since these peaks arise from ν(As−OFe) (*vide infra*). The increase in the intensity of the peak around 910 cm^{-1} suggests the formation of bidentate complexes, which is assigned to ν(As═O). This peak is observed for fully protonated MMA at pD 3 (Figure S3).

There are limited spectroscopic studies on the nature of MMA surface complexes on metal oxides. Cox and Ghosh[29] assumed inner-sphere complex formation for both MMA and DMA on hydrous ferric oxide and activated alumina based on ionic strength-dependent studies and SCM. Using extended X-ray absorption fine structure spectroscopy (EXAFS), Jing and co-workers[30] showed the formation of inner-sphere bi- and monodentate complexes for MMA and DMA, respectively, on

DOI: 10.1021/la504581p
Langmuir 2015, 31, 2749−2760

nanocrystalline TiO_2. Shimizu et al.[31] utilized ATR-FTIR and EXAFS and concluded that both organoarsenicals form bidentate−binuclear complexes with amorphous aluminum oxide (AAO). Hence, based on the above analysis, spectra shown in Figure 1 for adsorbed MMA at pH 7 suggest the formation of mostly monodentate MMA with some bidentate complexes. Increasing the temperature decreases the intensity of the 795 cm^{-1} feature along with an increase in the intensity of the feature at 872 cm^{-1}, which could be indicative of the preference to form mostly monodentate at the expense of bidentate surface complexes.

In addition, the lower panel in Figure 1 shows spectra of adsorbed DMA with most pronounced features at 837 and 798 cm^{-1}. At lower concentrations, the feature at 868 cm^{-1} is visible which is enveloped by the more intense neighboring band centered at 837 cm^{-1}. There is little effect of temperature on the intensity and shape of the broad bands at temperatures below 25 °C. When the temperature is increased to 35 and 50 °C, the frequency and intensity of the high frequency component at 876 cm^{-1} increase, and the intensity of the low frequency at 798 cm^{-1} decreases. These shifts suggest changes to surface speciation with temperature. We reported[20] earlier simultaneous formation of inner- and outer-sphere adsorbed DMA species, which gave rise to spectral components in the range 700−880 cm^{-1}. The spectral component at 798 is assigned to ν(As−O···H) from uncomplexed As−O bonds involved in strong H-bonding as observed for DMA in the solid phases.[28] This component has contributions from ν(As−OFe) from inner-sphere complexes. The component at 837 cm^{-1} is assigned to ν(As═O) from free As═O groups, with bond order of ca. 1.5. Moreover, components at 868 and 876 cm^{-1} are assigned to ν(As═O) in outer-sphere complexes as a result of the involvement of the second As−O group in DMA in strong H-bonding that decreased electronic delocalization. Based on the above analysis, it can be inferred that increasing the temperature increases the number of outer-sphere complexes evident by the increase in the intensity of the high-frequency spectral component and decreases the number of inner-sphere complexes evident by the decrease in the low-frequency component. Such clear response to temperature increase is not observed for arsenate, which confirms our earlier interpretation of kinetic and thermodynamic results that increasing organic substitution on arsenate increases the number of weakly bonded surface complexes.[8,32]

Binding Constants from the Langmuir Adsorption Isotherm Model and the Triple-Layer SCM as a Function of Temperature. Figure 3 shows experimental adsorption isotherm data collected for arsenate, MMA, and DMA at pH 7 as a function of temperature. These isotherms were generated by plotting the baseline−line corrected heights of the spectral feature in Figure 1 as a function of concentration. As shown in Figure 3, these peak heights were also converted to surface coverage in units of molecules/cm^2. For comparison, adsorption isotherms were also generated from peak areas (not shown). However, because of the dependency of the penetration depth of the IR light on wavelength in spectra collected using ATR-FTIR, it is challenging to derive a model that converts peak areas to surface coverage.[32] To extract thermodynamic equilibrium binding constants, two models were applied: the simple 1-site Langmuir model and the triple-layer SCM because of their extensive use in arsenic research as summarized in the Introduction. Also, the triple-layer SCM was chosen for its ability to consider both inner- and outer-sphere complexes. The equation of the former is $\theta_X = K_{eq}[X]/(1 + K_{eq}[X])$, where θ_X is the fractional surface coverage of species X at equilibrium with its concentration in solution.[33] The former was applied to isotherm data generated from peak heights and peak areas. The solid lines in the left panel of Figure 3 are the least-squares fitting results of the 1-site Langmuir model to the experimental data. Best-fit values of K_{eq} are listed in Table S4 from fits applied also to isotherms generated from features below 800 cm^{-1}. The same data analysis procedure was applied to isotherms generated from peak areas, and best-fit K_{eq} values are listed in Table S5. A later section describes the extraction of thermodynamic state functions from the temperature dependence of these values. When incorporating the standard deviation from experimental data, the triple-layer SCM model was well able to describe the arsenate adsorption data using one inner-sphere bidentate surface complexation constant, MMA adsorption using a mixture of bidentate and protonated monodentate inner-sphere surface complexation constants, and the DMA adsorption data using one inner-sphere and one outer-sphere monodentate surface complexation constants (see Figure 3). The quality of the fit, as measured by the overall variance V_y = SOS/DF, where SOS is the weighted sum of squares of the residuals and DF is the degrees of freedom was excellent for all model fits. Values of V_y are presented in Table S6. The smaller the value of V_y, the closer the fit of the model to the experimental data. The standard deviations listed in Table S6 are between 1 and 4% of log K values, except for inner-sphere DMA. The standard deviations of these particular constants are so large because the inner-sphere DMA surface species is present at much lower concentrations than the outer-sphere DMA surface species. In the case of 5 °C this is 1/100th, and in the cases of 35 and 50 °C it is 1/10th. When running the model without the inclusion of inner-sphere DMA surface species, the goodness-of-fit criterion V_y changed by an average of 0.08 from the results with inner-sphere DMA surface species shown in Table S6. These results reproduce recent experimental findings from kinetic measurements of DMA desorption behavior relative to arsenate.[32] Therefore, calculation of thermodynamic state functions described in the following section will be limited to outer-sphere DMA surface species.

It is important to note that the aforementioned log K values for surface complexes were extracted using intrinsic log K values at 25 °C for reactions S7−S10 in the Supporting Information assuming minimal change in these values with temperature. In order to test if this assumption is reasonable, the temperature dependence of log K for reactions S7−S10 and S15−S17 were calculated from the reported enthalpies listed in Table S3 of the Supporting Information. The triple-layer SCM was run again to extract values of log K^{is}_{iAs} as a function of temperature. Table 1 lists uncorrected versus corrected log K^{is}_{iAs} using values listed in Table S3 as input parameters. The model was only able to optimize the neutral surface complex when the standard deviations of the adsorbed arsenic amounts were included. Including the temperature dependence of the log K values leaves the arsenate adsorption log K unchanged. More importantly, the adsorbed arsenate amounts are identical in all digits (not shown here). This result may be because one log K in the protonation−dissociation constant pair increases while the other one decreases thus minimizing the change in PZC. The same is true for the background electrolyte log Ks. Hence, in the absence of temperature-dependent log K information on

DOI: 10.1021/la504581p
Langmuir 2015, 31, 2749−2760

Table 1. Effect of Temperature Corrections of log *K* Values for Reactions S7−S10 and S15−S17 in the Supporting Information on the Output of Fitting the Triple-Layer SCM to the Arsenate Adsorption Isotherm Data

temp (°C)	log K^{is}_{iAs}	V_y	log K^{is}_{iAs}	V_y
	uncorrected		corrected	
5	12.91 ± 0.09	0.6	13.05 ± 0.09	0.6
15	13.09 ± 0.05	0.6	13.18 ± 0.05	0.6
25	12.93 ± 0.06	0.4	12.99 ± 0.06	0.4
35	13.00 ± 0.02	3.0	13.00 ± 0.02	3.0
50	13.02 ± 0.07	0.6	13.01 ± 0.07	0.6

the dissociation of organoarsenicals, it is reasonable to carry out the modeling with the 25 °C log *K* values.

For comparison with previous modeling studies conducted at room temperature, the charge distribution multisite complexation (CD-MUSIC) model was used to describe bidentate surface complexes of arsenate adsorption on goethite[34,35] and akagenéite (β-FeOOH).[36] Hering and Dixit[37] summarized findings from diffuse layer model (DLM) and constant capacitance model (CCM) for arsenite and arsenate adsorption on suspensions of iron and aluminum (oxyhydr)oxides where mononuclear innersphere complexes gave the best fits. The CD-MUSIC model was used to describe the adsorption of methylated arsenicals on nanocrystalline titanium oxide,[30] where bidentate and monodentate surface complex configurations were incorporated in the model to describe MMA and DMA, respectively. Earlier, Cox and Ghosh used the triple-layer SCM to describe the adsorption of methylated arsenicals on hydrous ferric oxide, where it was necessary to assume innersphere complexation on two sets of reactive surface sites having differing adsorption affinities.[29] Our temperature-dependent modeling study is the first to extract changes in adsorption enthalpy and entropy from SCM results from incorporating reactions consistent with spectroscopic observations.

Enthalpy and Entropy of Arsenicals Ligand Exchange Reactions with Sites on Hematite Nanoparticles from Mathematical Models. The above section described in detail how K_{eq} values were extracted from applying the 1-site Langmuir model and triple-layer SCM to the experimental data. Values of K_{eq} from the Langmuir model were converted to ΔG°_{ads} at each temperature using the relation $\Delta G^{\circ}_{ads} = -RT \ln(55.5\ \mathrm{M}\cdot K_{eq})$, where the 55.5 M is the concentration of liquid water, R is the gas constant, and T is temperature in kelvin. For K_{eq} values from the triple-layer SCM, they were multiplied by either 55.5 M or $(55.5\ \mathrm{M})^2$ in order to cancel the concentration units listed in eqs S2−S6. According to the van't Hoff equation, ΔG°_{ads} is related to the enthalpy and entropy of adsorption

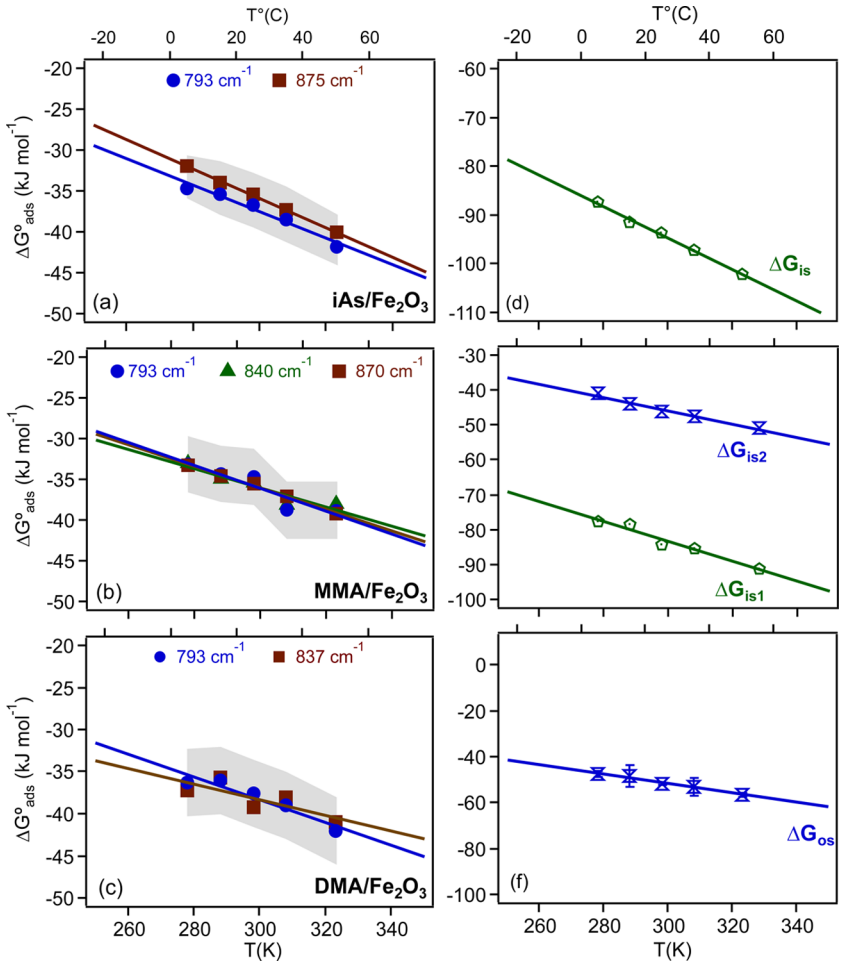

Figure 4. Temperature dependence of ΔG°_{ads} calculated from the Langmuir equilibrium constants, K_{eq}, listed in Table S4 (filled markers, left panel), and log K_{eq} values from the triple-layer SCM listed in Table S6 (empty markers, right panel). The solid lines are linear least-squares fitting. According to the van't Hoff equation, the slope equals $-\Delta S^{\circ}_{ads}$ and the y-intercept equals ΔH°_{ads}, which are listed in Table 2. The shaded areas represent $\pm\sigma$.

DOI: 10.1021/la504581p
Langmuir 2015, 31, 2749−2760

Table 2. Thermodynamic State Functions for the Adsorption of Arsenicals on Hematite from Temperature-Dependent Adsorption Isotherms Generated from the Analysis of Peak Heights

spectral data (cm^{-1})	875		840		837	
compound	arsenate		MMA		DMA	
model	1-site Langmuir[a]	SCM[b]	1-site Langmuir[a]	SCM[b]	1-site Langmuir[a]	SCM[b]
ΔH_{ads} (kJ mol^{-1})	+18	+2.0 ± 0.8 (is)	−0.8	+2.3 ± 0.9 (is1) +11 ± 4 (is2)	+2.3	+9.8 ± 5 (os)
ΔS_{ads} (kJ K^{-1} mol^{-1})	+0.18	+0.29 ± 0.03 (is)	+0.11	+0.29 ± 0.03 (is1) +0.19 ± 0.02 (is2)	+0.14	+0.20 ± 0.02 (os)

[a]Estimation of uncertainty is shown in Figure S5. [b]2SOH site model with 2 × $[SOH]_{max}$. See Schematic 1 for pictorial representation of these complexes. Estimation of uncertainty was propagated from standard deviation values in log K values listed in Table S6 of the Supporting Information.

through $\Delta G^{\circ}_{ads} = \Delta H^{\circ}_{ads} - T\Delta S^{\circ}_{ads}$. The left panel in Figure 4 shows the linear dependency of ΔG°_{ads} on T calculated from the Langmuir K_{eq} values as a function of spectral components for arsenate, MMA, and DMA adsorption on hematite nanoparticles. A similar graph was generated from fits to peak area adsorption isotherms (Figure S4). Table 2 and Table S7 list the ΔH°_{ads} and ΔS°_{ads} values for each arsenical from analyzing the most intense spectral feature and peak area isotherms, respectively.

Results shown in Table 2 from applying the SCM model predict endothermic adsorption of all three arsenicals. The Langmuir model predicts an exothermic adsorption of MMA on hematite nanoparticles. When using the peak area for analysis in extracting thermodynamic functions (Table S7), results predict endothermic adsorption for arsenate and MMA and exothermic for DMA. There is no clear trend in ΔH°_{ads} values using these models that would provide insights into the effect of organic substitution on arsenate. Values of log K for bidentate arsenate and MMA are on the same order and smaller by a factor of 5 than values for monodentate MMA and outer-sphere DMA. Using DFT calculations, we recently reported values for ΔG°_{ads}, ΔH°_{ads}, and ΔS°_{ads} at room temperature for the adsorption of hydrated arsenate on iron oxide clusters.[9] The ΔG°_{ads} and ΔH°_{ads} for the formation of bidentate binuclear arsenate complex was calculated to be −46 and −57 kJ mol^{-1}, respectively, which are more negative than monodentate mononuclear complexes (−41.5 and −47 kJ mol^{-1}), respectively. Watts et al.[10] also calculated ΔG°_{ads} for the formation of arsenate bidentate binuclear complexes on iron clusters and found that they range from −74 to −54 kJ/mol using the B3LYP functional used by Adamescu et al.[9] As shown in detail below, experimentally measured heats of adsorption were exothermic for all three arsenicals studied herein, with arsenate releasing 1.6× more heat that methylated arsenicals.

In order to explain the net positive change in calculated ΔS°_{ads} listed in Table 2 and Table S7, reactions 1−5 show the release of water molecules upon complexation, which would result in +0.14 kJ K^{-1} mol^{-1} for reactions 1 and 2 and +0.07 for reactions 3 and 4 using the standard molar entropy of liquid water (0.07 kJ K^{-1} mol^{-1}).[38] Best-fit entropy values from the Langmuir model are close to this theoretical value, but those obtained from applying the triple-layer SCM to the experimental data are higher, suggesting additional contributions to positive ΔS°_{ads}. Reactions 1−5 suggest a net increase in the degrees of freedom in surface species (adsorbed arsenicals as products versus coordinated water as reactants), which from a statistical thermodynamics standpoint[39] would result in a net increase in the entropy of adsorption. As mentioned in the Introduction, an entropy change of −0.084 kJ K^{-1} mol^{-1} was reported by Tuna et al.[11] for arsenate adsorption on a hybrid Fe(III)-activated carbon adsorbent at pH 3, which was attributed to increased order during reaction and formation of stable complexes. Partey et al.[12] reported +0.033 kJ K^{-1} mol^{-1} at pH 7 for arsenate adsorption on laterite iron concretions with no clear explanation. Zeng attributed the positive ΔS°_{ads} (+0.013 kJ K^{-1} mol^{-1}) for arsenate adsorption on iron oxide/silica to increased disorder at the interface. For comparison with other systems, a positive ΔS°_{ads} (+0.44 kJ K^{-1} mol^{-1}) was calculated for the adsorption of europium(III) on hematite in the pH range from 3 to 7.[40] The primary contribution to this reaction entropy was attributed to the loss of water from the Eu(III) hydration sphere upon forming the bidentate surface complexes with hematite. Also, a net increase in ΔS°_{ads} (+0.22 and +0.42 kJ K^{-1} mol^{-1} depending on complex charge) was calculated for the adsorption of mellitic acid ($C_{12}H_6O_{12}$, benzenehexacarboxylic acid) onto goethite, which was explained by changes in hydration upon adsorption that lead to the liberation of water molecules.[41]

Using DFT calculations for arsenate adsorption,[9] reactions were constructed such that the number of reactants equal that of the products to minimize entropy. This was achieved by treating water leaving groups as a cluster instead of a monomer [i.e., $(H_2O)_6$ versus $6(H_2O)$], which is environmentally relevant since surface water would likely to leave the surface and hydrogen bond with surrounding water molecules in the first solvation shell. This is consistent with the recent work by Watts et al.[10] that calculated ΔS_{ads} for arsenate adsorption on model iron (oxyhyr)oxide clusters, where configurational entropy terms were neglected. In light of these calculations and the above summary of literature from batch experiments, it can be concluded that arsenicals adsorption on hematite will result in a net positive change in entropy due to disturbances in the hydration shells of solvated species and the oxide interface.

When using the Langmuir model, the variation in the slope and intercept values depends to a lesser degree on which spectral component is analyzed than on the uncertainty in ΔG°_{ads}. In Figure S5, the resulting variability in ΔH°_{ads} and ΔS°_{ads} from applying the Langmuir model is quantified for the three arsenicals investigated herein. While minimum variations exist for ΔG°_{ads} and ΔS°_{ads} (slope of the lines), values of ΔH°_{ads} span about 20 kJ mol^{-1}, from slightly exothermic to mostly endothermic. For data from the SCM (Table S6), the uncertainty in the log K values is less than 1−4% for all arsenicals except inner-sphere DMA (*vide supra*). When these values are propagated to uncertainty in ΔG°_{ads}, the size of the error bars is similar to the width of the markers used in the right panel of Figure 4. This suggests that the variability in ΔH°_{ads} and ΔS°_{ads} is much smaller than that from the Langmuir

DOI: 10.1021/la504581p
Langmuir 2015, 31, 2749−2760

model. Therefore, when it comes to choosing a model to quantify the adsorption energies, it is more accurate to use log K values from SCMs that best describe the binding mechanism under equilibrium. In the next section, the discrepancy in values and uncertainties of energy values from different models is discussed in the context of measured adsorption energies using microcalorimetry.

Enthalpy of Arsenicals Ligand Exchange Reactions with Sites on Hematite Nanoparticles from Microcalorimetric Measurements. Figure 5 shows the raw data

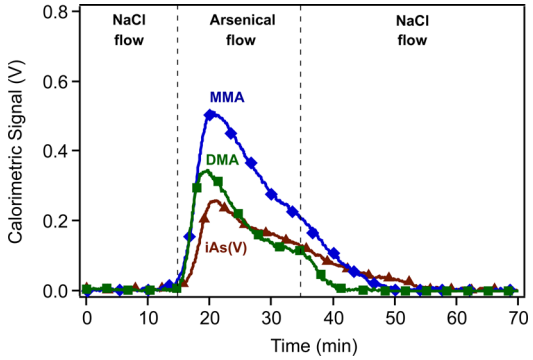

Figure 5. Calorimetric response obtained for the adsorption of arsenate, MMA, and DMA onto hematite nanoparticles. An increase in voltage resulting in a positive peak corresponds to a release of energy and hence an exothermic reaction.

(electrical response versus time) for flowing arsenical solutions over hematite nanoparticles followed by flowing the background NaCl solution. Using the calibration curve in the Supporting Information (Section 5) and the amounts of arsenic adsorbed for each species, the total heats of reaction were transformed into ΔH_{ads} in units of kJ/mol (Table 3), which is

Table 3. Summary of Experimental Energies and Molar Enthalpies Corresponding to the Adsorption of iAs, MMA, and DMA on Hematite Nanoparticles

	energy released (mJ/g)	measured ΔH°_{ads} (kJ/mol)
arsenate	509	−160
MMA	2601	−85
DMA	974	−102

technically not a standard state enthalpy. The amount of arsenic adsorbed was taken as the difference between the total mass injected and the mass recovered from effluent samples collected only during the arsenic treatment phase, including the return of the calorimetric signal to baseline in 10 mM NaCl. Values of ΔH_{ads} were calculated to be −85, −102, and −160 kJ mol^{-1} for MMA, DMA, and arsenate, respectively. The difference between MMA and DMA (17 kJ/mol) is 1.6−1.9 times smaller than that of arsenate, which is consistent with an adsorption process dominated by bidentate for the latter.

As shown in Figure 5 and calculated in Table 3, the reaction of all three arsenicals (arsenate, MMA, and DMA) species with the hematite nanoparticles is exothermic, consistent with previous studies using microcalorimetry to study oxyanions sorption on metal oxides. For example, arsenate adsorption on Al(III)-(hydr)oxides was found to be exothermic and with heats ranging from −40 to −60 kJ/mol.[16] Similarly, Harvey and Rhue[14] determined average ΔH_{ads} for phosphate adsorption onto mixed Al(III)−Fe(III) oxides to be −35 kJ/mol. For this data, using the total heats generated per sorption event and the actual experimental mass corresponding to each arsenic injection, the normalized energy were 2601, 974, and 509 mJ/g for MMA, DMA, and arsenate, respectively (see Table 3). Because of the complexity of the adsorption mechanism governing each arsenic molecule, this method of normalization may not be totally accurate from a thermodynamic standpoint, namely relative to ΔH°_{ads}. In other words, the experimental challenge of matching surface site saturation with "heat" evolution for weakly adsorbing species such as DMA limits interpretation to total energies. This is not surprising since the microcalorimetry experiments performed herein provide measurements for the average behavior of adsorption on particles, which is different from temperature-programmed desorption experiments using single crystal surface with well-defined surface planes.

Assuming ΔS°_{ads} = +0.14 kJ K^{-1} mol^{-1} based on discussion in the above section, the ΔH_{ads} listed in Table 3 could be converted to ΔG_{ads} for arsenate, MMA and DMA: −202, −127, and −144 kJ mol^{-1}, respectively. Our results indicate a lower adsorption affinity for MMA and DMA compared to iAs by a factor of ∼1.5. This observation is consistent with trends in ΔG°_{ads} of these arsenic compounds on hematite nanoparticles shown in the right panel of Figure 4 from applying the triple-layer SCM and those reported earlier by Cox and Ghosh[29] and Lafferty and Loeppert.[42] The results also align with the observations of Zhang et al.,[43] who found that the replacement of one or two hydroxyls from the arsenate molecule with methyl (CH_3) groups as in the case of MMA and DMA species reduces the arsenic adsorption affinity at pH values below 7 when goethite was used as a model oxide. For example, at pH 4, the authors observed a 55% decrease in DMA uptake compared with arsenate, but only a 4% reduction was recorded for MMA adsorption. The authors speculated that the low affinity of DMA to goethite was due mainly to the formation of monodentate rather than bidentate surface complexes typically observed for oxyanion adsorption. Similar trends were observed by Shimizu et al.[31] on amorphous aluminum oxides, where less MMA and DMA, 78 and 15%, were adsorbed within 5 min compared to 100% arsenate. These results were explained by dynamic stereochemistry, where fewer hydroxyl groups on methylated arsenicals results in lower probability for the formation of the most thermodynamically favorable molecular orientation on the surface.

Using the total energies of the calorimetric peaks associated with the nitrate displacement of exchangeable chloride (NO_3^-/Cl^-) before and after the arsenate treatment (Table 4), some differences were observed in the potential mechanism underlying the adsorption behavior of the three arsenicals with hematite nanoparticles. The NO_3^-/Cl^- exchange on clean metal oxide surfaces is a completely reversible process. Calorimetric peak areas, and hence energies, for each of the cycles of NO_3^-/Cl^- and Cl^-/NO_3^- are consistently measured to be within 5% of each other.[14,44,45] Hence, this anion exchange reaction can be used as a probe of any changes to the surface positive charge as a result of a more permanent and/or stronger complexation mechanism. For instance, Harvey and Rhue[14] measured an irreversible decrease in peak areas of anion exchange pre- and post-phosphate adsorption on Al(III) and Fe(III) oxides and arsenate on Al(III) (hydr)oxides, respectively. They interpreted this observation to indicate that phosphate and arsenate were irreversibly adsorbed onto

DOI: 10.1021/la504581p
Langmuir 2015, 31, 2749−2760

Table 4. Comparison of the Energies (mJ) Associated with NO_3^-/Cl^- Exchange on Hematite Nanoparticle Last Pretreatment and First Post-Arsenic Treatment[a]

arsenical species	last pretreatment	first posttreatment	energy change[b] (%)
iAs(V)	1.86	0.04	97.8
MMA	2.20	1.01	54.10
DMA	5.70	4.53	20.52

[a]Energies of exchange in this table are listed as positive numbers, although NO_3^- replacing Cl^- is exothermic. The last pretreatment and first postreatment column represents the energy of only the nitrate replacing chloride portion of the complete ion exchange cycle. [b]The energy change is calculated as $(\text{energy}_{\text{pretreatment}} - \text{energy}_{\text{posttreatment}})/\text{energy}_{\text{pretreatment}} \times 100$.

ion exchange sites, hence causing the sites to no longer participate in charge development. Utilizing a similar approach of comparing the peak areas of ion exchange pre- and post-sulfate sorption on boehmite nanoparticle, Appel et al.[44] found that of the 79% decrease in ion exchange peak areas postsulfate treatment on Al(III) (hydr)oxides, only 61% decrease was permanent after several NO_3^-/Cl^- and Cl^-/NO_3^- exchange cycles. The authors postulated that the large decrease in surface positive charge immediately after sulfate adsorption seemed to result from both inner- and outer-sphere surface complexation. The subsequent 18% increase of surface positive charge resulted from the loss of the outer-sphere sulfate complexes in the $NaNO_3$ and NaCl flow streams, demonstrating that *in situ* surface charge measurement by flow microcalorimetry can provide valuable insights into the underlying sorption mechanism and various pools of complexes formed.

Our experimental observations have shown that immediately following arsenate adsorption, the surface positive charge, as measured by the energy of NO_3^-/Cl^- exchange, had decreased significantly by 97.8%, to ~2% of its pre-arsenate treatment quantity (Table 4). In contrast, both MMA and DMA showed a lesser effect on the surface positive charge, which was reduced by 54.1% and 20.5%, respectively. Given that the first post-treatment energy was measured after the flow of background NaCl solution subsequent to each arsenic treatment, the energy change seems to indicate that arsenate is forming more irreversible complexes than MMA and DMA since complexes of arsenate are not being flushed away by the NaCl flow. These findings align with the IR data described above, demonstrating that arsenate has a larger number of bidentate surface complexes relative to monodentate or outer sphere observed for MMA and DMA. The outer sphere and monodentate complexes will be more likely to desorb from the hematite nanoparticle surface in the NaCl background solution.

CONCLUSIONS AND SIGNIFICANCE

Spectroscopic data reported herein coupled with experimentally measured heats of adsorption highlight that arsenate surface complexes are mostly dominated by bidentate, MMA by a mixture of mono- and bidentate, and DMA by mostly outer sphere. The application of the empirical Langmuir model and the triple-layer SCM to temperature-dependent isotherm data derived from ATR-FTIR spectra predicted an endothermic adsorption process. Using microcalorimetry, exothermic adsorption heats for all three arsenicals studied herein were obtained with arsenate releasing 1.6−1.9 times more heat than methylated arsenicals. The latter experimental measurements are consistent with previous work and results from DFT calculations. While applying the models did not yield the correct sign for adsorption heats, one advantage of applying them was extracting values for the positive change in the entropy of adsorption, which were similar among the three arsenicals investigated. Contributions to the increase of entropy are originating from the displacement of surface water molecules and the increase in the size of surface species upon arsenicals adsorption.

Our findings are significant as they constitute systematic experimental and modeling investigations of methylated arsenicals interactions with hematite nanoparticles under environmentally relevant conditions. While the synthetic hematite nanoparticles used herein do not necessarily match those formed in nature, the chemistry at the aqueous/solid interface of these particles is on average representative of the surface chemistry of other iron(oxyhydr)oxide materials. These results could be translated to applications in water filtration by incorporating speciation as a factor in the modeling and design of efficient arsenic removal technologies. They also shed light into the dynamic methylation/demethylation of arsenic commonly observed in the environment, even under anaerobic conditions.[46] Because of the documented association of arsenate and methylated arsenicals with iron (oxyhydr)oxides in soils,[47] our study suggests that these associations do not occur with similar energetics, and hence, the likelihood for demethylation is high under the right redox and microbial conditions. This study further highlights three key areas of further investigation: the need to measure log *K* values for acid dissociation of DMA and MMA as a function of temperature to improve the set of input data in the triple-layer SCM, the need for standardizing the procedure for calorimetric measurements of adsorption heats to minimize discrepancies in the literature, and comparing thermodynamics of arsenicals surface interactions with hematite formed through other processes and other Fe-bearing phases.

ASSOCIATED CONTENT

Supporting Information

Figures and tables showing detailed analysis. This material is available free of charge via the Internet at http://pubs.acs.org.

AUTHOR INFORMATION

Corresponding Author

*Phone (519) 884-0710, ext 2873; fax (519) 746-0677; e-mail halabadleh@wlu.ca (H.A.A.).

Notes

The authors declare no competing financial interest.

ACKNOWLEDGMENTS

H.A.A. acknowledges partial funding from Laurier, NSERC, and Early Researcher Award from Ontario's Ministry of Research and Innovation. N.K. acknowledges the support of the U.S. Department of Energy (DOE) Office of Science Early Career Research Program Grant No. 211267.

REFERENCES

(1) Ravenscroft, R.; Brammer, H.; Richards, K. *Arsenic Pollution: A Global Synthesis*; Wiley-Blackwell: Malden, MA, 2009.

(2) Mudhoo, A.; Sharma, S. K.; Garg, V. K.; Tseng, C. H. Arsenic: An Overview of Applications, Health, and Environmental Concerns and Removal Processes. *Crit. Rev. Environ. Sci. Technol.* **2011**, *41*, 435−519.

DOI: 10.1021/la504581p
Langmuir 2015, 31, 2749−2760

(3) Hayakawa, T.; Kobayashi, Y.; Cui, X.; Hirano, S. A New Metabolic Pathway of Arsenite: Arsenic−Glutathione Complexes Are Substrates for Human Arsenic Methyltransferase Cyt19. *Arch. Toxicol.* **2005**, *79*, 183−191.
(4) Cullen, W. R. *Is Arsenic an Aphrodisiac? The Sociochemistry of an Element*; RSC Publishing: Cambridge, 2008.
(5) Fengxiang, X. H.; Su, Y.; Monts, D. L.; Plodinec, M. J.; Banin, A.; Triplett, G. E. Assessment of Global Industrial-Age Anthropogenic Arsenic Contamination. *Naturwissenschaften* **2003**, *90*, 395−401.
(6) Yu, M.; Long, Y.-Z.; Sun, B.; Fan, Z. Recent Advances in Solar Cells Based on One-Dimentional Nanostructure Arrays. *Nanoscale* **2012**, *4*, 2287−2796.
(7) Sparks, D. L. Metal and Oxyanion Sorption on Naturally Occurring Oxide and Clay Mineral Surfaces. In *Environmental Catalysis*; Grassian, V. H., Ed.; Taylor & Francis Group: Boca Raton, FL, 2005; pp 3−36.
(8) Tofan-Lazar, J.; Al-Abadleh, H. A. ATR-FTIR Studies on the Adsorption/Desorption Kinetics of Dimethylarsinic Acid on Iron-(Oxyhydr)oxides. *J. Phys. Chem. A* **2012**, *116*, 1596−1604.
(9) Adamescu, A.; Hamilton, I. P.; Al-Abadleh, H. A. Density Functional Theory Calculations on the Complexation of *p*-Arsanilic Acid with Hydrated Iron Oxide Clusters: Structures, Reaction Energies and Transition States. *J. Phys. Chem. A* **2014**, *118*, 5667−5679.
(10) Watts, H. D.; Tribe, L.; Kubicki, J. D. Arsenic Adsorption onto Minerals: Connecting Experimental Observations with Density Functional Theory Calculations. *Minerals* **2014**, *4*, 208−240.
(11) Tuna, A. Ö.; Özdemir, E.; Simsek, E. B.; Beker, U. Removal of As(V) from Aqueous Solution by Activated Carbon-Based Hybrid Adsorbents: Impact of Experimental Conditions. *Chem. Eng. J.* **2013**, *223*, 116−128.
(12) Partey, F.; Norman, D.; Ndur, S.; Nartey, R. Arsenic Sorption onto Laterite Iron Concretions: Temperature Effect. *J. Colloid Interface Sci.* **2008**, *321*, 493−500.
(13) Zeng, L. Arsenic Adsorption from Aqueous Solutions on an Fe(III)-Si Binary Oxide Adsorbent. *Water Qual. Res. J. Can.* **2004**, *39*, 267−275.
(14) Harvey, O. R.; Rhue, R. D. Kinetics and Energetics of Phosphate Sorption in a Multi-Component Al(III)−Fe(III) Hydr(oxide) Sorbent System. *J. Colloid Interface Sci.* **2008**, *322*, 384−393.
(15) Groszek, A. J. Flow Adsorption Microcalorimetry. *Thermochim. Acta* **1998**, *312*, 133−143.
(16) Kabengi, N. J.; Daroub, S. H.; Rhue, R. D. Energetics of Arsenate Sorption on Amorphous Aluminum Hydroxides Studied Using Flow Adsorption Calorimetry. *J. Colloid Interface Sci.* **2006**, *297*, 89−94.
(17) Penn, C. J.; Warren, J. G. Investigating Phosphorus Sorption onto Kaolinite Using Isothermal Titration Calorimetry. *Soil Sci. Soc. Am. J.* **2009**, *73*, 560−568.
(18) Penn, C. J.; Zhang, H. Isothermal Titration Calorimetry as an Indicator of Phosphorus Sorption Behavior. *Soil Sci. Soc. Am. J.* **2010**, *74*, 502−511.
(19) Miltenburg, J. C.; Golterman, H. L. The Energy of the Adsorption of *o*-Phosphate onto Ferric Hydroxide. *Hydrobiologia* **1998**, *364*, 93−97.
(20) Mitchell, W.; Goldberg, S.; Al-Abadleh, H. A. In-Situ ATR-FTIR and Surface Complexation Modeling Studies on the Adsorption Thermodynamics of Mono- and Di-Substituted Organoarsenicals on Iron-(Oxyhydr)oxides. *J. Colloid Interface Sci.* **2011**, *358*, 534−540.
(21) Herbelin, A.; Westall, J. C. *FITEQL: A Computer Program for Determination of Chemical Equilibrium Constants from Experimental Data. Rep. 6-01, Version 4.0*; Department of Chemistry, Oregon State University, Corvallis, OR, 1999.
(22) Myneni, S. C. B.; Traina, S. J.; Waychunas, G. A.; Logan, T. J. Experimental and Theoretical Vibrational Spectroscopic Evaluation of Arsenate Coordination in Aqueous Solutions, Solids, and at the Mineral-Water Interfaces. *Geochim. Cosmochim. Acta* **1998**, *62*, 3285−3300 and references therein.
(23) Goldberg, S.; Johnston, C. T. Mechanisms of Arsenic Adsorption on Amorphous Oxides Evaluated Using Macroscopic Measurements, Vibrational Spectroscopy, and Surface Complexation Modeling. *J. Colloid Interface Sci.* **2001**, *234*, 204−216.
(24) Roddick-Lanzilotta, A. J.; McQuillan, A. J.; Craw, D. Infrared Spectroscopic Characterization of Arsenate (V) Ion Adsorption from Mine Waters, Macraes Mine, New Zealand. *Appl. Geochem.* **2002**, *17*, 445−454.
(25) McAuley, B.; Cabaniss, S. Quantitative Detection of Aqueous Arsenic and Other Oxoanions Using Attenuated Total Reflectance Infrared Spectroscopy Utilizing Iron Oxide Coated Internal Reflection Elements to Enhance the Limits of Detection. *Anal. Chim. Acta* **2007**, *581*, 309−317 and references therein.
(26) Catalano, J. G.; Park, C.; Fenter, P.; Zhang, Z. Simultaneous Inner- and Outer-Sphere Arsenate Adsorption on Corundum and Hematite. *Geochim. Cosmochim. Acta* **2008**, *72*, 1986−2004.
(27) Loring, J. S.; SAndstrom, M. H.; Noren, K.; Persson, P. Rethinking Arsenate Coordination at the Surface of Goethite. *Chem.—Eur. J.* **2009**, *15*, 5063−5072.
(28) Cowen, S.; Duggal, M.; Hoang, T. N.; Al-Abadleh, H. A. Vibrational Spectroscopic Characterization of Some Environmentally-Important Organoarsenicals: A Guide for Understanding the Nature of Their Surface Complexes. *Can. J. Chem.* **2008**, *86*, 942−950.
(29) Cox, C. D.; Ghosh, M. M. Surface Complexation of Methylated Arsenates by Hydrous Oxides. *Wat. Res.* **1994**, *28*, 1181−1188.
(30) Jing, C.; Meng, X.; Liu, S.; Baidas, S.; Patraju, R.; Christodoulatos, C.; Korfiatis, G. P. Surface Complexation of Organic Arsenic on Nanocrystalline Titanium Oxide. *J. Colloid Interface Sci.* **2005**, *290*, 14−21.
(31) Shimizu, M.; Ginder-Vogel, M.; Parikh, S. J.; Sparks, D. L. Molecular Scale Assessment of Methylarsenic Sorption on Aluminum Oxide. *Environ. Sci. Technol.* **2010**, *44*, 612−617.
(32) Tofan-Lazar, J.; Al-Abadleh, H. A. Kinetic ATR-FTIR Studies on Phosphate Adsorption on Iron-(Oxyhydr)oxides in the Absence and Presence of Surface Arsenic: Molecular-Level Insights into the Ligand Exchange Mechanism. *J. Phys. Chem. A* **2012**, *116*, 10143−10149.
(33) Masel, R. I. *Principles of Adsorption and Reaction on Solid Surfaces*; John Wiley & Sons: New York, 1996.
(34) Antelo, J.; Avena, M.; Fiol, S.; Lopez, R.; Arce, F. Effects of pH and Ionic Strength on the Adsorption of Phosphate and Arsenate at the Goethite−Water Interface. *J. Colloid Interface Sci.* **2005**, *285*, 476−486.
(35) Stachowicz, M.; Hiemstra, T.; Van Riemsdijk, W. H. Surface Speciation of As(III) and As(V) in Relation to Charge Distribution. *J. Colloid Interface Sci.* **2006**, *302*, 62−75.
(36) Kersten, M.; Karabacheva, S.; Vlasova, N.; Branscheid, R.; Schurk, K.; Stanjek, H. Surface Complexation Modeling of Arsenate Adsorption by Akagenéite (*β*-FeOOH)-Dominant Granular Ferric Hydroxide. *Colloids Surf., A* **2014**, *448*, 73−80.
(37) Hering, J. G.; Dixit, S. Contrasting Sorption Behavior of Arsenic(III) and Arsenic(V) in Suspensions of Iron and Aluminum Oxyhydroxides. In *Advances in Arsenic Research: Integration of Experimental and Observational Studies and Implications for Mitigation*; O'Day, P. A., Vlassopoulos, D., Meng, X., Benning, L. G., Eds.; ACS Symposium Series; American Chemical Society: Washington, DC, 2005; Vol. *915*, pp 8−24.
(38) Atkins, P. W.; de Paula, J. *Physical Chemistry*, 7th ed.; W.H. Freeman and Company: New York, 2008.
(39) McQuarrie, D. A. *Statistical Thermodynamics*; Harper & Row Publishers: New York, 1973.
(40) Estes, S. L.; Arai, Y.; Becker, U.; Fernando, S.; Yuan, K.; Ewing, R. C.; Zhang, J.; Shibata, T.; Powell, B. A. A Self-Consistent Model Describing the Thermodynamics of Eu(III) Adsorption onto Hematite. *Geochim. Cosmochim. Acta* **2013**, *122*, 430−447.
(41) Angove, M. J.; Wells, J. D.; Johnson, B. B. The Influence of Temperature on the Adsorption of Mellitic Acid onto Goethite. *J. Colloid Interface Sci.* **2006**, *296*, 30−40.
(42) Lafferty, B. J.; Loeppert, R. H. Methyl Arsenic Adsorption and Desorption Behavior on Iron Oxides. *Environ. Sci. Technol.* **2005**, *39*, 2120−2127.

DOI: 10.1021/la504581p
Langmuir 2015, 31, 2749−2760

(43) Zhang, J. S.; Stanforth, R. S.; Pehkonen, S. O. Effect of Replacing a Hydroxyl Group with a Methyl Group on Arsenic (V) Species Adsorption on Goethite (α-FeOOH). *J. Colloid Interface Sci.* **2007**, *306*, 16−21.
(44) Appel, C.; Rhue, R. D.; Kabengi, N. J.; Harris, W. Calorimetric Investigation of the Nature of Sulfate and Phsophate Sorption on Amorphous Aluminum Hydroxide. *Soil Sci.* **2013**, *178*, 180−188.
(45) Kabengi, N. J.; Rhue, R. D.; Daroub, S. H. Using Flow Calorimetry to Determine the Molar Heats of Cation and Anion Exchange and the Point of Zero Charge on Amorphous Aluminum Hydroxides. *Soil Sci.* **2006**, *171*, 13−21.
(46) Dombrowski, P. M.; Long, W.; Farley, K. J.; Mahony, J. D.; Capitani, J. F.; Di Toro, D. M., Thermodynamic Analysis of Arsenic Methylation. *Environ. Sci. Technol.* **2005**, *39*.
(47) Shimizu, M.; Arai, Y.; Sparks, D. L. Multiscale Assessment of Methylarsenic Reactivity in Soil. 2. Distribution and Speciation in Soil. *Environ. Sci. Technol.* **2011**, *45*, 4300−4306.

DOI: 10.1021/la504581p
Langmuir 2015, 31, 2749−2760